Phys. Status Solidi B **252,** No. 7, 1656–1663 (2015) / **DOI** 10.1002/pssb.201552234

physica status solidi b
www.pss-b.com
basic solid state physics

Carbon allotropes exhibiting negative linear compressibility

Jean Paul Formosa[1], Reuben Cauchi[2], and Joseph N. Grima[*,1,2]

[1] Department of Chemistry, Faculty of Science, University of Malta, Msida MSD2080, Malta
[2] Metamaterials Unit, Faculty of Science, University of Malta, Msida MSD2080, Malta

Received 17 April 2015, revised 2 June 2015, accepted 4 June 2015
Published online 6 July 2015

Keywords carbon allotropes, hexagonal honeycomb structures, negative compressibility

[*] Corresponding author: e-mail auxetic@um.edu.mt, Phone: +356 23402274

Negative linear compressibility, i.e., the phenomenon of expansion rather than shrinkage in at least one direction upon the application of a hydrostatic compressive pressure is an unusual mechanical property which is attracting more interest in the recent years. Here, through analysis of published data by Hu et al. [J. Superhard Mater. **36**, 257–269 (2014)] as well as through static force-field based simulations, it is shown that it is possible to achieve this property in the novel carbon allotropes built from sp^2 and sp^3 hybridized carbon atoms which have a two-dimensional projection that resembles a honeycomb motif in their (001) plane. This is in accordance with earlier predictions that honeycombs deforming through a hinging-like mechanism could exhibit this property for certain geometries.

1 Introduction The discovery of new carbon allotropes such as buckyballs, nano-tubes, and graphene, has intrigued several chemists and materials scientists to further study new forms of carbon. The unique electrical and thermal properties and the high strength and hardness in the case of covalently bonded carbon networks lead to the advent in development of superior materials with very specific applications. Carbon based systems also represent some of the earlier systems to be studied *vis-à-vis* their potential to exhibit anomalous mechanical behavior. Such properties include auxeticity i.e., the phenomenon of becoming wider rather than thinner when uniaxially stretched (negative Poisson's ratio) [1], as well as negative linear compressibility i.e., the phenomenon of expanding in at least one direction when hydrostatically compressed. The fields of auxeticity [2–25, 47] and negative compressibility [26–38] have been gaining significant growth in the last decades, partly in view of the scientific curiosity of having materials and model systems which exhibit such counter intuitive mechanical properties, as well as the wide range of applications where such materials can be used.

Various nanoscale materials which exhibit negative linear compressibility have been identified [31, 34–38]. Here it should be noted that negative compressibility as a result of pressure being exerted by a fluid on a solid system can be achieved via two modes. The first, relates to scenarios where the pressure is exerted by the fluid particles on the external surface of a non-porous solid system [31, 32, 34, 35]. In this case, negative compressibility generally arises due to very high positive Poisson's ratios and anisotropy. On the other hand negative compressibility can also be achieved in porous solid systems as a result of the fluid particles exerting a pressure both from within the pores of the material and on its surface, altering the relative orientation of the structural features in the system, which may result in NLC [44–45]. At the nanoscale it is more common to have negative linear compressibility being manifested as a result of the former effect. Several highly anisotropic geometrical based models have been proposed so as to explain the occurrence of this anomalous property. Such models include the wine-rack and conventional honeycomb mechanisms; two systems which can be highly anisotropic and exhibit very high positive Poisson's ratios in particular directions leading to the possibility of negative compressibility.

In fact earlier work [32] shows that idealized hexagonal honeycombs such as the ones in Fig. 1 deforming solely through a hinging-like mode of deformation can show negative linear compressibility (NLC) for a given set of initial angles [32]. The ratio of h/l, (i.e., the ratio of the length of the ribs along the vertical direction and the inclined ribs) determines the range of angles where negative compressibility is shown with smaller h/l ratios favoring

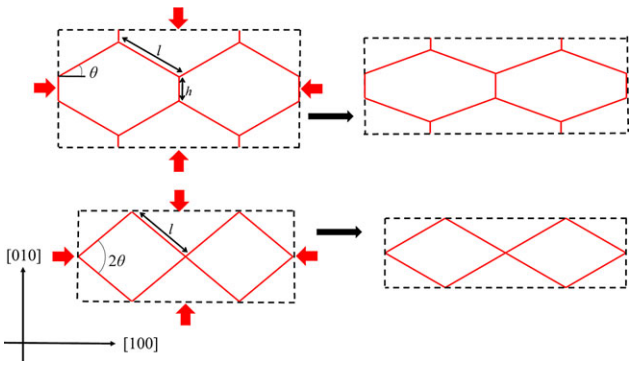

Figure 1 Negative linear compressibility from 2D non-re-entrant honeycomb systems and the particular case of 2D wine-rack-like systems. Note that in both cases the maximum NLC behavior is measured in the [100] direction [32].

more negative values of linear compressibility in the Ox_1 direction. It was also shown that all non-re-entrant idealized hinging honeycombs are expected to exhibit a negative compressibility along the horizontal Ox_2 direction for $\theta > 45^\circ$ [32]. This range can be further increased by increasing h/l, although the actual magnitudes of the negative linear compressibility decrease. However, it is seldom the case that a real system deforms through a single mode of deformation, and any such additional mode could either augment, or, more likely, decrease the extent of NLC [32]. For example, if the honeycomb system shown in Fig. 1 would have also deformed though changes in length of the various ligaments (stretching mechanism), then the extent of NLC would decrease, potentially even be totally annulled [32, 46].

This work will look at two all-carbon networks, recently proposed by Hu et al. [39] which have a characteristic honeycomb-like motif in their nanostructure, a geometry which, as noted above, is well known for its potential to exhibit negative compressibility. These novel all-carbon systems were predicted using the newly developed USPEX and CALYPSO methods based on *ab initio* simulations. This seminal work has shown that these graphyne derived networks are energetically more stable than the corresponding graphyne under ambient pressure while most of the proposed networks are more stable than fullerene C_{60}. Hu et al. have also shown that these networks can attain high hardness while also showing tuneable electronic properties, and that the formation of these networks from the corresponding graphyne exhibits a lower barrier than the graphite to diamond transformation. In addition they have also calculated the elastic constants for single crystals of these systems [39]. This, together with the resemblance that particular planes of such system bear to hexagonal honeycombs have prompted the reported work, where their compressibility properties are analyzed, particularly their potential to exhibit NLC. Static force-field based simulations are also performed in an attempt to obtain additional evidence through an independent modelling methodology that these windows of NLC do indeed exist. With the same method, an attempt is also made to simulate the nanolevel deformations that occur when these crystals are hydrostatically compressed. Such behavior is explained through geometry based mechanistic models that are supported through detailed static force-field base simulations of these systems under hydrostatic loading conditions.

2 Methodology Static force-field based simulations were performed on two all-carbon networks (Fig. 2) as described by Hu et al. which networks can be described as three-dimensional (3D) polymers of graphyne sub-structures [39]. In particular the first of these networks, henceforth referred to as oC24, is described by an orthorhombic unit cell containing 24 atoms. The geometric arrangement of these atoms is in such a way that the system resembles layers of non-planar hexagonal honeycombs parallel to the (001) plane as shown in Fig. 2. These layers are connected to one another with single and double bonds forming smaller hexagonal honeycombs perpendicular to the (001) plane. For such a 3D network, the projection in the (001) plane is comparable to a honeycomb of non-re-entrant hexagonal cells with a twofold rotational symmetry. The second network contains 16 atoms in a unit cell having hexagonal symmetry thus referred to as hP16, and is similar to the aforementioned network; however, it has regular honeycombs in the (001) plane exhibiting hexagonal symmetry including the characteristic rotational symmetry of order 6 [39].

The simulations were performed using the Materials Studio 8.0 molecular modelling software provided by Accelrys. For both systems a $1 \times 1 \times 1$ unit cell was used which was aligned in such a way so that its [001] crystallographic direction was aligned parallel to the z global axis, the [010] direction was constrained to lie in the yz-plane and the [100] direction was left unconstrained. In all cases no further symmetry constraints were used in the simulations i.e., all atoms in the system were not restricted to adopt positions dictated by the expected symmetry apart from those imposed from periodicity. The unit cell size was

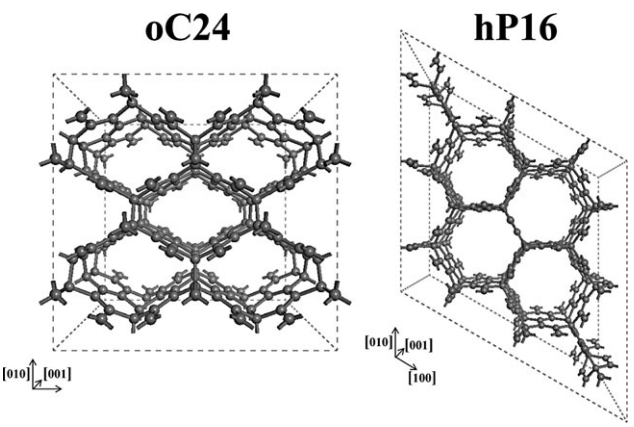

Figure 2 Perspective views of (001) planes of the hP16 and oC24 networks constructed from the coordinates as simulated by Hu et al. [39].

deemed to be sufficiently large to adequately model the structural mechanical properties of these systems following a validation study using larger unit cell sizes.

Both systems were simulated using an energy expression based on the Dreiding force-field [40] which has been extensively used for many years to study such carbon based systems [31, 41] including studies which were aimed to assess negative Poisson's ratios and/or negative compressibility behavior, as well as the more recently developed PCFF forcefield which has also been used on similar systems [31, 41, 42]. In the case of the Dreiding forcefield, partial charges were calculated using the Charge Equilibration procedure as developed by Rappe et al. [43]. For both force fields, the non-bond interactions were summed up using the EWALD summation convention. Systems were optimized to the default Materials Studio 8.0 convergence criteria to less than $0.0001\,\mathrm{kcal\,mol^{-1}\ A^{-1}}$ using the SMART minimizer integrated in Materials Studio 8. The fractional atomic positions as well as the unit cell parameter of the systems obtained were then compared to those obtained via *ab initio* methods by Hu et al. [39]. Also the elastic constants c_{ij} which relate stress σ to strain ε according to $\sigma = [c_{ij}]\varepsilon$ were calculated from the second derivative of the energy expression since

$$c_{ij} = \frac{1}{V}\frac{\partial^2 E}{\partial\varepsilon_i \partial\varepsilon_j}, \quad i,j = 1,2,...,6,$$

where E is the energy expression, V is the volume of the unit cell, $\varepsilon_2 = \varepsilon_y$, and $\varepsilon_3 = \varepsilon_z$ are the strains in the x, y, and z directions, respectively, while, $\varepsilon_5 = \gamma_{xz}$ and $\varepsilon_6 = \gamma_{xy}$ are the shear strains in the yz, xz, and xy planes, respectively.

Off-axis mechanical properties including the Poisson's ratios and linear compressibility were then calculated from both sets of force-field simulated elastic constants as well as from the *ab initio* results by Hu et al. [39]. These were analyzed so as to identify any negative Poisson's ratio and negative compressibility that may be present.

Additional simulations were also carried by both force-fields to simulate changes in the nanostructure of these networks under hydrostatic compression. These simulations were performed in ten incremental steps up to a maximum hydrostatic pressure which causes a change of *ca.* 2% in the most amenable dimension. In particular, assuming that a hydrostatic pressure p_{max} is required to cause a hydrostatic compression of 2%, the optimized system as obtained above was firstly re-minimized under the condition of an applied hydrostatic pressure of $p_{max}/10$ up to the default high convergence criteria, as described above. Once convergence was achieved, an additional pressure of $p_{max}/10$ was added, i.e., a total pressure of, and the process repeated again and again until a total pressure of p_{max} was reached. Measurements of the various parameters which describe the geometry of the system were then performed on each of the optimized structures at the different levels of hydrostatic pressures in an attempt to identify the nano-level deformations which are occurring when the systems are hydrostatically compressed.

3 Results and discussion The unit cell parameters for both systems studied here as simulated by the Dreiding and PCFF force-fields are listed in Table 1 where they are compared with the respective data obtained by Hu et al. trough *ab initio* simulations [39]. A comparison of the fractional coordinates is also provided in the Tables S1 and S2 in the Supporting Information. This data clearly shows that both force-fields can simulate very well, at least when compared to the much more computationally intensive *ab initio* simulations, the structure and properties of these all-carbon networks. Furthermore, as illustrated in Fig. 3 which shows the projections of (001) planes of the simulated networks compared to those by Hu et al., the expected geometry features including, the honeycomb motif in the (001) are being adequately simulated. Ensuring that the structures are simulated adequately constitutes an extremely important part of the validation process which should precede any simulation of the elastic constants since it is well known that the mechanical properties depend significantly on the structure being modelled. Obviously, had the simulation resulted in unrealistic networks, any further simulations on the elastic constants would have been futile.

The elastic constants as simulated by these force-fields are tabulated in Table 2 and the calculated off-axis linear compressibility properties are graphically represented in Fig. 4, where they are also compared to those obtained from the analysis of the data via *ab initio* simulations by Hu et al. [39]. A comparison of this data suggests that although the actual magnitudes of the elastic constants may differ depending on the method used, the trends observed are rather similar. The agreement in these trends is very important as it suggests that any qualitative deductions drawn on this data are independent of the method used hence unlikely to be an artefact of these simulations. For example the compressibility properties in the (001) plane of the hP16 system which projects as a regular hexagon are such that all sets of data suggest that the system is completely isotropic in this plane with constant positive compressibility behavior. Here it must be emphasised that this behavior is to be expected since structures exhibiting hexagonal symmetry are expected to exhibit in-plane isotropy.

Table 1 Unit cell parameters as simulated for both systems studied here as simulated by the Dreiding and PCFF force-fields and the results obtained by Hu et al., using *ab initio* simulations [39].

	a (Å)	b (Å)	c (Å)	α (°)	β (°)	γ (°)
hP16						
Hu et al.	6.777	6.777	4.219	90	90	120
Dreiding	6.843	6.843	4.298	90	90	120
PCFF	6.855	6.855	4.134	90	90	120
oC24						
Hu et al.	6.974	6.485	4.195	90	90	90
Dreiding	6.836	6.904	4.304	90	90	90
PCFF	6.899	6.716	4.205	90	90	90

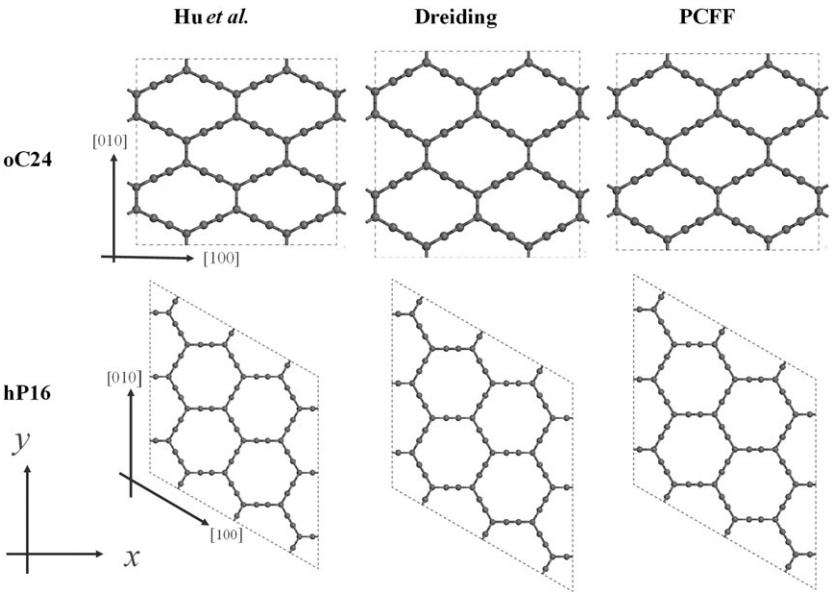

Figure 3 Projections of (001) planes of the hP16 and oC24 networks simulated using the Dreiding and PCFF force-fields and those simulated by Hu et al. [39].

In the case of the oC24 system it is evident that all three simulation methods give the same profile for the variation of the linear compressibility in the (001) plane against direction of measurement. In all cases, the minimum linear compressibility occurs along the [100] direction where a negative value is measured. Maximum positive compressibility is observed along the [010] direction. This is very significant as the projection of the oC24 network in the (001) plane can be described in terms of a non-regular hexagonal honeycomb, characterized by the parameters illustrated in Fig. 5, which geometry is well known for its potential to exhibit negative compressibility, if the honeycomb deforms primarily through hinging deformation. In fact the off-axis compressibility trends are in concordance with predictions of this proposed model. Table 3 lists the equivalent values of these geometric parameters where no external hydrostatic pressure is applied. From these measurements it becomes clear that through a previously developed analytical model [32] the geometry exhibited by the hP16 system could not have exhibited negative compressibility, even had the projection in the (001) plane deformed through idealized hinging. In fact, the geometry of this system lies outside the geometries for which negative compressibility is permitted by the analytical model. This is not the case for the oC24 system, where the geometry is within the required range for an idealized system to exhibit negative compressibility in the horizontal direction.

In an attempt to verify whether the negative compressibility in the system is indeed the result of such a deformation mechanism, measurements of various geometric parameters which describe the shape and size of these projected honeycombs as they change with an increase in the hydrostatic compression were made. These were compared to the equivalent measurements of the hP16 network (Fig. 5). This analysis of the manner of how the projected systems in the (001) plane deform upon the introduction of hydrostatic pressure shows that in the oc24 system, a hinging-type mechanism is indeed the most dominant mode of deformation as shown in **ANIM01.gif** in the Supporting Information.

Table 2 Elastic constants as simulated for both systems studied here as simulated by the Dreiding and PCFF force-fields and the results obtained by Hu et al., using *ab initio* simulations [39]. Note that the Dreiding force-field tends to overestimate the elastic constants although their relative ratios are approximately in conformity with the published work by Hu et al. and the results of PCFF force-field.

	c_{11}	c_{22}	c_{33}	c_{44}	c_{55}	c_{66}	c_{12}	c_{13}	c_{23}
hP16									
Hu et al.	254.0	–	764.2	200.8	–	–	197.8	71.7	–
Dreiding	335.9	–	935.8	195.7	–	–	232.5	143.5	–
PCFF	250.2	–	712.9	166.8	–	–	189.7	65.5	–
oC24									
Hu et al.	617.1	182.6	1009.0	149.3	392.2	133.4	216.4	149.0	42.2
Dreiding	676.9	287.3	1218.9	184.0	326.6	166.6	307.5	241.1	141.0
PCFF	541.9	201.6	824.8	164.0	289.3	159.7	250.9	107.0	65.9

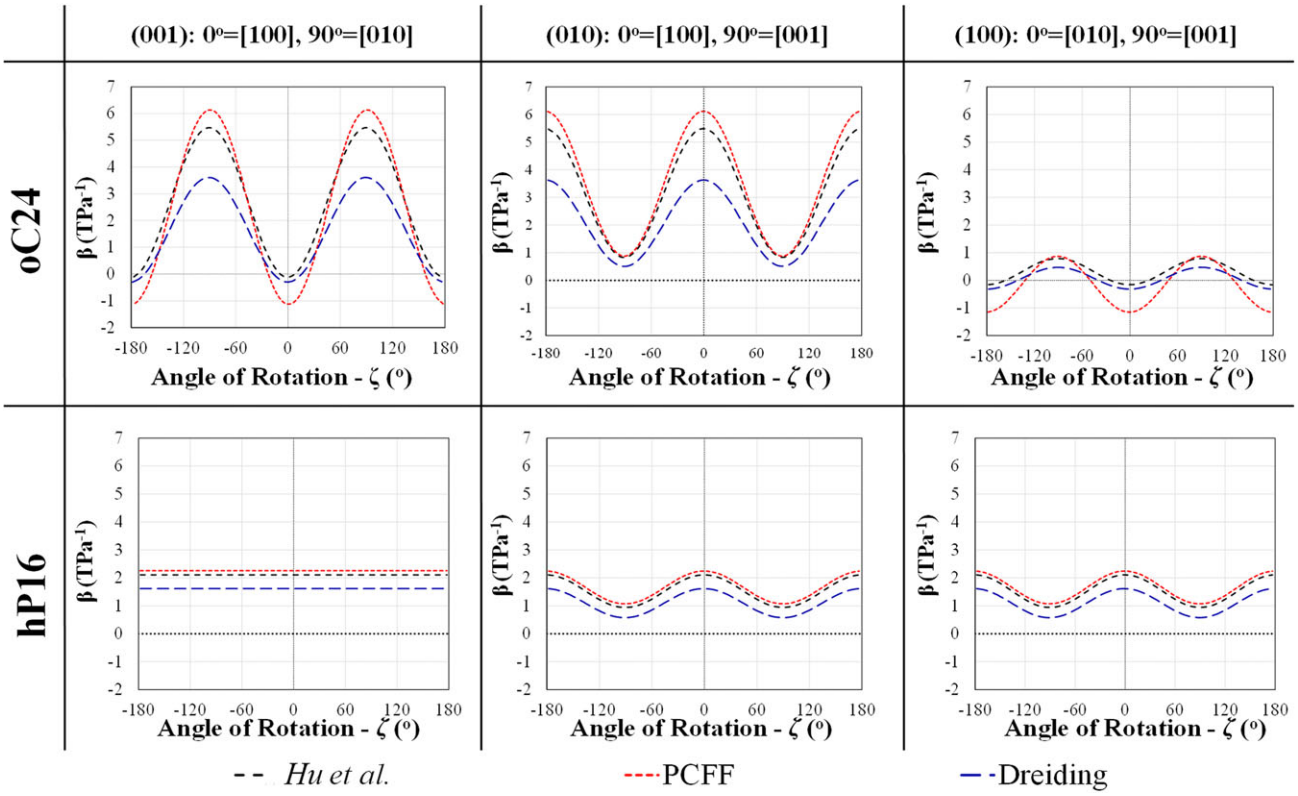

Figure 4 Calculated off-axis linear compressibility plots for the hP16 and oC24 networks as simulated using the Dreiding and PCFF forcefield compared with the results obtained by Hu et al., using *ab initio* simulations [39].

Figure 6 shows how the parameters X_1 and X_2 (which represent the horizontal and vertical projections of the honeycomb unit cell), the values for l_i ($i = 1, 2, \ldots, 7$) and h_j ($j = 1, 2, 3$) (which represent the various vertical and inclined rib lengths, respectively) and values for θ_k ($k = 1, 2, \ldots, 6$) (which represent the angles inside the projected honeycomb) change with application of hydrostatic pressure. Note that in all cases the property being measured is changing in a continuous manner indicating that the increments in pressure are not large enough so as to perturb the system or produce non-equilibrium states. In the case of the oC24 system, there is a very significant increase in value of θ_5 and θ_6 combined with the decrease in values of θ_1–θ_4. This will translate into an increase in the value of X_1, hence the NLC behavior in the x-direction. The values for θ_1, θ_2, θ_3, and θ_4 decrease to the same extent while θ_5 and θ_6, increase significantly by an equal amount as hydrostatic pressure is applied. The NLC behavior observed along the [100] direction qualitatively matches the conclusion from a previously developed

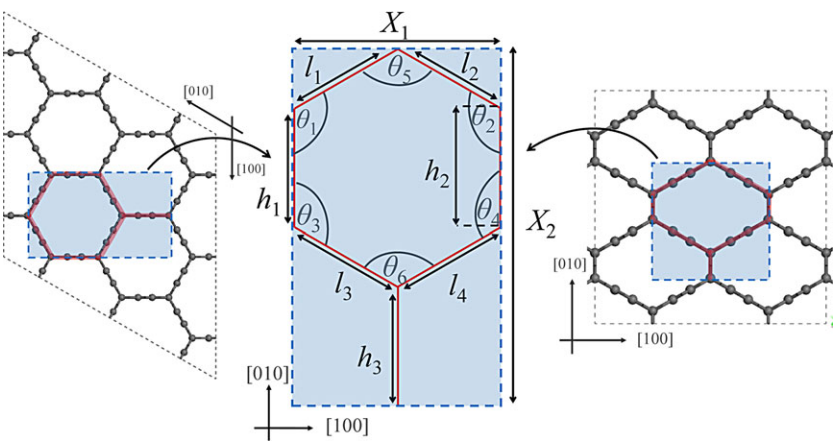

Figure 5 Figure showing the parameters X_1 and X_2 representing the horizontal and vertical projections of the honeycomb unit cell, the values for l_i and h_j representing the various vertical and inclined rib lengths, respectively, and values for θ_k representing the angles inside the projected honeycomb. Note that one set of data for each reading was plotted for both systems since all the values of l_i and, all the values for h_j change to a similar extent, respectively, while θ_1 and θ_5 represent values for θ_1–θ_4 and θ_5–θ_6, respectively.

Table 3 Values for the hP16 and oC24 systems of the geometric parameters h, l, and θ influencing the linear compressibility behavior, as described through a previously developed analytical model [32].

	h (Å)	l (Å)	θ (°)
hP16			
Hu et al.	3.913	3.913	30.0
Dreiding	3.951	3.951	30.0
PCFF	3.957	3.957	30.0
oC24			
Hu et al.	1.569	3.868	26.4
Dreiding	1.509	3.932	29.6
PCFF	1.433	3.943	29.2

analytical model [32] for a system with a similar h/l ratio and set of initial angles. A closer inspection of this oC24 system, however, suggests that this nanonetwork does not deform solely through idealized hinging, a result which is to be expected as the network studied here is much more complex in construction and the 2D honeycomb visualized in the (001) plane is a mere 2D projection of much more complex 3D network. In fact, an analysis of this 2D projection of the framework suggests that there is also some degree of change in the length of the ribs of the system which contributes to conventional positive compressibility properties. The net result is a system exhibiting a less negative value for compressibility then if the structure had to deform solely by hinging.

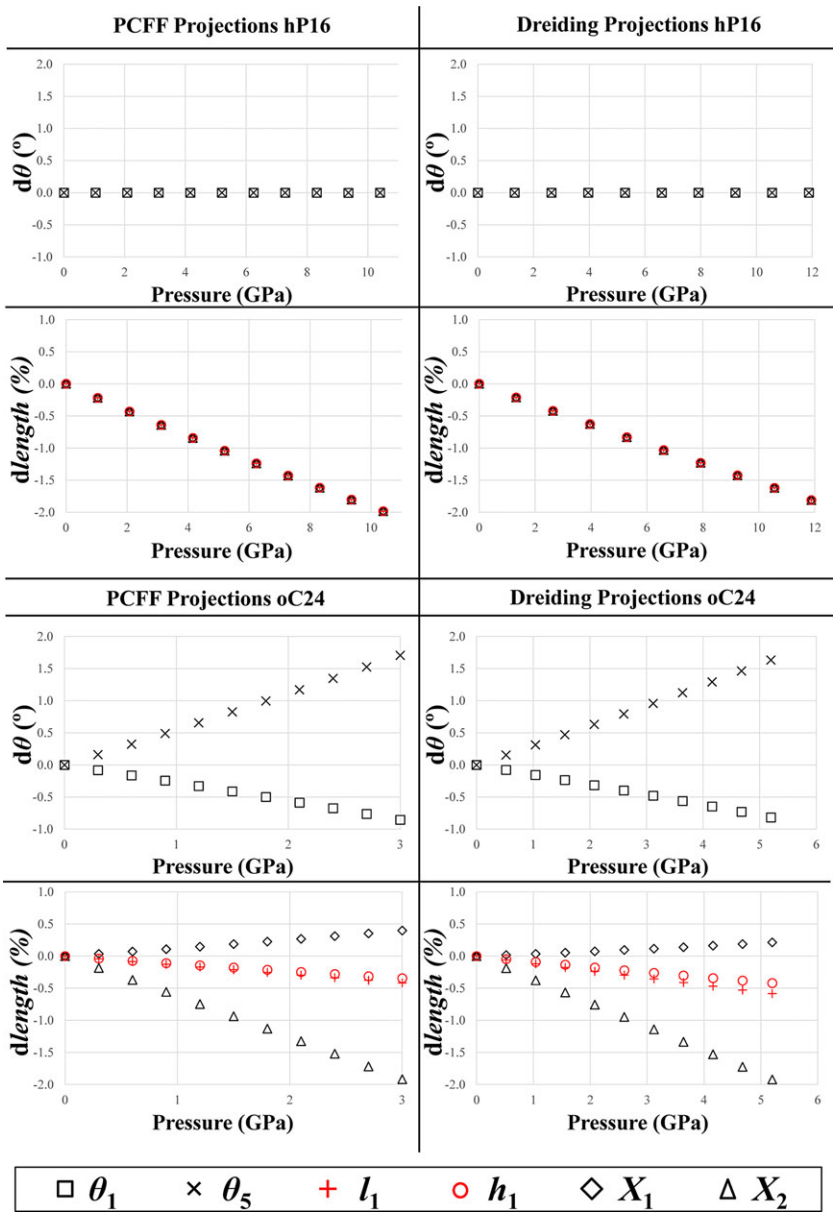

Figure 6 Graphs showing the changes in θ_1, θ_5, l_1, h_1, X_1, and X_2 with increasing hydrostatic pressure until a change of ca. 2% in the most amenable direction of the system as modelled with the Dreiding and PCFF forcefields for both systems studied.

In the case of the hP16 network, which exhibit positive isotropic compressibility properties in the (001) plane, there are no measurable changes in the angles θ_1–θ_6. Yet, there is a decrease in all the values of h and l which is of the same extent as the decrease in the parameters X_1 and X_2 as shown in Fig. 6. Consequently one can conclude that the 2D projected image of this network in the (001) plane may be describable through a stretching-like deformation mechanism which predominates in the hP16 network and hence it is unable to exhibit any NLC behavior as shown in **ANIM02.gif** in the Supporting Information.

All this is extremely remarkable as it confirms that nanocarbon networks which have 2D projections, describable through hexagonal centro-symmetric honeycombs can indeed be designed so as to exhibit the compressibility behavior predicted by the analytical models, including NLC. Obviously, these effects observed here are in fact not directly relatable to the two-dimensional projection of the network in the (001) plane but are the effect of more complex changes in the three-dimensional geometry of the systems which is made up of sp^3 and sp^2 hybridized carbon atoms. Thus all of the changes that are being measured in the 2D projection should be interpretable in terms of changes in the different C–C bond lengths, C–C–C bond angles, and C–C–C–C torsion angles. In fact if one looks in directions which are orthogonal to the (001) plane, one would find that what projects as a "rib" in the (001) plane is in fact a complex nanonetwork containing a set of smaller honeycombs, most of which are made up of 6-membered rings which also deform under hydrostatic pressure. By considering the changes in the internal angles of these aforementioned 6-membered rings, which constitute to the length of the ribs forming the honeycomb motif in the (001) plane one can determine the resultant effect of the change in angle over the lengths of the ribs projected in the (001) plane. In fact a contraction of such angles will inevitably lead to a decrease in the length of the projected ribs. The hP16 network does not exhibit NLC due to the fact that all the angles decrease in order to accommodate the stretching mechanism which predominates in the system.

To some extent, the same effect is also manifested in the oC24 network which together with some changes in torsion angles, and bond length changes leads to some degree of shortening of the projected horizontal ribs of length l upon application of pressure. As a result, the ribs are no longer perfectly straight and thus have to contract in order to accommodate this type of deformation. However, in this case there is also some very significant changes in the C–C–C angles which fall on a vertex of the honeycomb in the (001) plane and these changes lead to the NLC behavior. It is remarkable that, despite all the changes which to some extent hinder the hinging mechanism, negative compressibility is still exhibited, thus highlighting the robustness of this mechanism to generate NLC behavior. Had the shrinkage in the lengths of the honeycomb's sides not been present, then one would have expected that the extent of negative compressibility observed could have been even more pronounced. This was in fact confirmed through the use of a modified version of the Dreiding force-field which simply restricted C–C bond stretching through a tenfold increment in the stiffness of the C–C bond which resulted in an increase in the NLC in the [100] direction by *ca.* 170% that obtained by the unmodified Dreiding forcefield.

Before concluding it is important to note that the work presented here based on the results of simulations which, irrespective of how complex they may be, they would always need to be verified through experimental work. In fact it should be emphasized that the main aim of the current work is primarily to elucidate in a qualitative manner how the systems proposed by Hu et al. exhibit their particular, and, in some case anomalous, compressibility properties. In this respect, the actual values of the individual elastic constants as simulated in this study are likely to be just an approximation of the real values exhibited by these systems. Nevertheless given that, the same conclusion *vis-à-vis* the negative compressibility characteristics may be drawn from this study as well as the results obtained by Hu et al., it is likely that this negative linear compressibility effect will be manifested by these systems should they be synthesized. Should such networks indeed be synthesized, they would also most likely benefit from additional interesting characteristics such as very high conductivity down the [001] direction due to the extensive delocalization present. These systems are also likely to benefit from other interesting mechanical properties including some degree of auxeticity (evident from the data present if one had to look at the off-axis Poisson's ratio plots in the non-(001) planes). All this will hopefully provide an impetus to experimentalists to attempt further study these carbon allotropes.

4 Conclusions In this work it was shown that the oC24 carbon allotrope network proposed by Hu et al. [39] is predicted to exhibit NLC in the [100] direction. This finding was confirmed through simulations performed using the Dreiding and PCFF force-fields as well from an analysis of the original data by Hu et al. The force field based simulations of this systems under hydrostatic pressure have confirmed that the observed NLC is the result of a hinging honeycomb mechanism which is hindered to some extent by the concurrent operation of a stretching honeycomb mechanism. It was also found that a similar network did not exhibit NLC properties as in this case the geometry was not amenable, in accordance with the previous predictions [32]. All this has further established the robustness of this hinging honeycomb mechanism to generate NLC behavior and re-highlighted the very strong link between nanolevel geometry and nanoscale deformation mechanisms, and the macroscopic mechanical properties.

Supporting Information

Additional supporting information may be found in the online version of this article at the publisher's website.

References

[1] K. E. Evans, M. A. Nkansah, I. J. Hutchinson, and S. C. Rogers, Nature **253**, 124–124 (1991).
[2] R. H. Baughman, J. M. Shacklette, A. A. Zakhidov, and S. Stafstrom, Nature **392**, 362–365 (1998).
[3] A. Alderson and K. E. Evans, Phys. Rev. Lett. **89**, 225503 (2002).
[4] K. L. Alderson, V. R. Simkins, V. L. Coenen, P. J. Davies, A. Alderson, and K. E. Evans, Phys. Status Solidi B **242**, 509–518 (2005).
[5] K. Bertoldi, M. C. Boyce, S. Deschanel, S. M. Prange, and T. Mullin, J. Mech. Phys. Solids **56**, 2642–2668 (2008).
[6] M. R. Dudek and K. W. Wojciechowski, J. Non-Cryst. Solids **354**, 4304–4308 (2008).
[7] L. Mizzi, D. Attard, A. Casha, J. N. Grima, and R. Gatt, Phys. Status Solidi B **251**, 328–337 (2014).
[8] R. Gatt, J. P. Brincat, K. M. Azzopardi, L. Mizzi, and J. N. Grima, Adv. Eng. Mater. **17**, 189–198 (2014).
[9] J. N. Grima, S. Winczewski, L. Mizzi, C. Grech, R. Cauchi, R. Gatt, D. Attard, K. W. Wojchiechowski, and J. Rybicki, Adv. Mater. **27**, 1455–1459 (2015).
[10] J. W. Jiang and H. S. Park, Nature Commun. **5**, 4727 (2014).
[11] R. S. Lakes, Science **235**, 1038–1040 (1987).
[12] G. Milton, J. Mech. Phys. Solids **40**, 1105–1137 (1992).
[13] J. W. Narojczyk, A. Alderson, A. R. Imre, F. Scarpa, and K. W. Wojciechowski, J. Non-Cryst. Solids **354**, 4242–4248 (2008).
[14] F. Scarpa, J. Giacomin, Y. Zhang, and P. Pastorino, Cell. Polym. **24**, 1–16 (2005).
[15] K. W. Wojciechowski, Mol. Phys. **61**, 1247–1258 (1987).
[16] K. W. Wojciechowski, Phys. Lett. A **137**, 60–64 (1989).
[17] J. W. Narojczyk and K. W. Wojciechowski, J. Non-Cryst. Solids **356**, 2026–2032 (2010).
[18] K. W. Wojciechowski, K. V. Tretiakov, and M. Kowalik, Phys. Rev. E **67**, 036121 (2003).
[19] R. H. Baughman and D. S. Galvao, Nature Lett. **365**, 735–737 (1993).
[20] R. Gatt, D. Attard, P. S. Farrugia, K. M. Azzopardi, L. Mizzi, J. P. Brincat, and J. N. Grima, Phys. Status Solidi B **251**, 321–327(2014).
[21] R. Gatt, D. Attard, J. I. Azzopardi, K. M. Azzopardi, A. Casha, J. Briffa, and J. N. Grima, Sci. Rep. **5**, 8395 (2015).
[22] R. Gatt, D. Attard, P. S. Farrugia, K. M. Azzopardi, L. Mizzi, J. P. Brincat, and J. N. Grima, Phys. Status Solidi B **250**, 2012–2019 (2013).
[23] G. Cicala, G. Recca, L. Oliveri, Y. Perikleous, F. L. Scarpa, C. Lira, A. Lorato, D. J. Grube, and G. Ziegmann, Compos. Struct. **94**, 3556–3562 (2012).
[24] T. Buckmann, R. Schittny, M. Thiel, M. Kadic, G. W. Milton, and M. Wegener, New J. Phys. **16**, 033032 (2014).
[25] C. He, P. Liu, A. C. Griffin, C. W. Smith, and K. E. Evans, Macromol. Chem. Phys. **206**, 233–239 (2005).
[26] V. V. Novikov and K. W. Wojciechowski, Exp. Theor. Phys. **95**, 462–471 (2002).
[27] V. V. Novikov and K. W. Wojciechowski, Phys. Status Solidi B **242**, 645–652 (2005).
[28] R. Lakes and K. W. Wojciechowski, Phys. Status Solidi B **245**, 545–551 (2008).
[29] T. Strek, B. Maruszewski, J. W. Narojczyk, and K. W. Wojciechowski, J. Non-Cryst. Solids **354**, 4475–4480 (2008).
[30] A. A. Pozniak, H. Kaminski, P. Kedziora, B. Maruszewski, T. Strek, and K. W. Wojciechowski, Rev. Adv. Mater. Sci. **23**, 169–174 (2010).
[31] R. H. Baughman, S. Stafstrom, C. Cui, and S. O. Dantas, Science **279**, 1522–1524 (1998).
[32] J. N. Grima, D. Attard, R. Caruana-Gauchi, and R. Gatt, Scr. Mater. **65**, 565–568 (2011).
[33] R. Gatt and J. N. Grima, Phys. Status Solidi B **245**, 236–238 (2008).
[34] A. B. Cairns, A. L. Thompson, M. G. Tucker, J. Haines, and A. L. Goodwin, J. Am. Chem. Soc. **134**, 4454–4456 (2012).
[35] A. L. Goodwin, D. A. Keen, and M. G. Tucker, Proc. Natl. Acad. Sci. USA **105**, 18708–18713 (2008).
[36] A. E. Aliev, J. Oh, M. E. Kozlov, A. A. Kuznetsov, S. Fang, A. F. Fonseca, and R. H. Baughman, Science **323**, 1575–1578 (2009).
[37] A. P. M. Barboza, H. Chacha, C. K. Oliviera, T. F. D. Fernandes, B. S. Archanjo, R. J. C. Batista, and B. R. A. Neves, Nano Lett. **12**, 2313–2317 (2012).
[38] A. B. Cairns, J. Catafesta, C. Levelut, J. Rouquette, A. van der Lee, L. Peters, A. L. Thompson, V. Dmitriev, J. Haines, and A. L. Goodwin, Nature Mater. **12**, 212–216 (2013).
[39] Y. Hu, M. Hu, J. He, Q. Wang, Q. Huang, D. Yu, and B. Xu, J. Superhard Mater. **36**, 257–269 (2014).
[40] S. L. Mayo, B. D. Olafson, and W. A. Goddard, J. Phys. Chem. **94**, 8897–8909 (1990).
[41] K. E. Evans, A. Alderson, and F. R. Christian, J. Chem. Soc., Faraday Trans. **91**, 2671–2680 (1995).
[42] J. N. Grima, C. Zerafa, and J. P. Brincat, Phys. Status Solidi B **251**, 375–382 (2014).
[43] A. K. Rappe and W. A. Goddard, J. Phys. Chem. **95**, 3358–3363 (1991).
[44] J. N. Grima, D. Attard, and R. Gatt, Phys. Status Solidi B **245**, 2405–2414 (2008).
[45] D. L. Barnes, W. Miller, K. E. Evans, and A. Marmier, Mech. Mater. **46**, 123–128 (2012).
[46] J. N. Grima, R. Caruana-Gauci, K. W. Wojciechowski, and K. E. Evans, Smart Mater. Struct. **22**, 084015 (2013).
[47] K. M. Azzopardi, J. P. Brincat, J. N. Grima, and R. Gatt, RSC Adv. **5**, 8974–8980 (2014).